Egypt. J. Geo. **Vol 66,** pp: 59-82 (2022)

Egyptian Journal of Geology
https://egjg.journals.ekb.eg

Utilization of Remote Sensing data in the mapping of the Cretaceous-Quaternary rocks, El Fayum-Greater Cairo region (south El Kattaniya high), Egypt

Abdel Nasser R. Abuzied[1], Ali M. Abd-Allah[2] and Abdelhay A. Farrag[3]
Geology Department, Faculty of science, New Valley Univ, Kharga, 72511, Egypt [1]
Geology Department, Faculty of science, Ain Shams Univ., Cairo, Egypt [2]
Geology Department, Faculty of science, Assuit Univ., Assuit, 71516 Egypt [3]

OVER the last few years, remote sensing techniques have become an indispensable in Earth science, especially in geological investigation. El Fayum-Greater Cairo region is characterized by strong diversity in the rocks lithologies (Upper Cretaceous-Quaternary units) and the affecting structures, as well as the agricultural activities at both sides of the Nile River in the Nile Valley and tow water lakes. These geologic diversities encourage us selecting this region to applying the PCA and ICA techniques for the Landsat 8 OLI and Sentinel-2A imagery data. These two applications are used to define the ratio combinations for each sedimentary lithologic facies and mixed facies, basaltic flows, agricultural systems, and water bodies of different salinity. Several geologic factors are determined controlling the quality appearances on the processed images, which are the lithologic homogeneity, percent of each lithology in the mixed facies, rock unit thickness, outcrop width, weathering intensity, surficial sediment covers, which part of the unit is exposed, and topographic occurrence of the unit. Three orders of qualities are suggested for the band combination ratios that used in the separation of limestone, limestone mixed facies, sand-sandstone, sandstone mixed facies, basaltic flows, clastic and carbonate mixed facies, agricultural cover, water bodies (Qarun and Wadi Rayan lakes and Nile River). These combination ratios are controlled by the lithologic homogeneity, percents of lithologies in the mixed facies, rock unit thickness, outcrop width, weathering intensity, surficial sediment covers, which part of the unit is exposed, and topographic setting of the unit. The Upper Eocene sandstone and claystone mixed facies are well represented on the ICA images rather than those on the PCA. The whole basaltic flows in the study area are discriminated well on most images whereas the large (thick) flow parts are separated only on the PCAL (6/5/3RGB) and ICAs (7/2/11RGB). The east-west faults that offseted the basaltic sheets are clearly mapped on the PCAL3/1/2RGB, ICAL3/1/2RGB, and ICAL4/7/3 images, as well as they are mapped on the ICAs11/2/12RGB and ICAs3/11/5RGB.

Keywords: Kattaniya high, Principal component analysis, independent principal component and geological setting.

Introduction

The area around Kattaniya high includes El Fayuom-Abu Roash district in the northeastern corner of Western Desert and the Cairo-east Bani Suef district lying in the north Eastern Desert. Both districts are separated by the Nile Valley (Fig. 1). This area has a wide diversity in the rock exposures in geologic ages and lithologic units, it includes the rock units belonging to Upper Cretaceous mainly carbonate, Eocene carbonate

*Corresponding author: nasserabuzied@yahoo.com
Received: 20/09/2022; Accepted: 18/10/2022;
DOI: 10.21608/EGJG.2022.164071.1023

and shale, Oligocene sand; gravels; and basalts, Miocene sand, and Pliocene-Quaternary clay and sand. These geological diversities encourage us to select this area as the target of the present study. The detailed geological mapping was carried out separately for some parts inside the study area, Moustafa et al. (1985) for the Cairo-Helwan part; Moustafa (1989) for the Abu Roash part; and Said (1979) for the El Fayum depression.

The mapping of the present rock units and the affecting structural elements is the main aim of the present study. This mapping is attended using the remote sensing processed data with carefully field investigation and measuring data. These data will be integrated to select the most significant band combinations can be used in the discrimination of each lithological unit as well as the linear structures (faults and folds). Because the eastern and western Nile have different lithological facies, it was necessary to discriminate the different rock types and determine their degree of similarity to compare and validate with field geological mapping. The present aim extends to also cover the analyses of the measured field data to produce a complete geologic map including different rock units exposed at both sides of the Nile Valley particularly for the Middle-Upper Eocene units. the effects of El Kattaniya high in the rock unit distribution and the affecting structures are also elucidated.

The present study area is located between latitudes 29° 08’ 40”N - 3\0° 03’ 23”N and longitudes 30°17’ 15”E - 31°35’ 20”E (Fig. 1).

Remote sensing is one of the most common and successful processes in exploring geology because of the importance of understanding the spatial distribution of geological mapping. Remote sensing is a powerful and important technique that can be used to improve the process of regional geological mapping (Pour and Hashim, 2015). The main aim of lithological mapping is to gain a better understanding of the spectral characteristics of a wide range of terrain (Grunsky et al., 2015).

Principle Component Analysis (PCA) and Independent Component Analysis (ICA) are the most important methods of remote sensing techniques which applied on Landsat -8 and Sentinel-2 multispectral imagery to achieve the objective of the present study. The resulted data and information were checked and verified using the field collected data.

Stratigraphy

One of the most factor had the attention of the present authors to the present area is the sever differences in the Eocene rocks units which are exposed at both sides of the Nile Valley (eastern and western sides of the study area) (Fig. 2).

In the western side of the study area, the oldest Upper Cretaceous stratigraphic units are

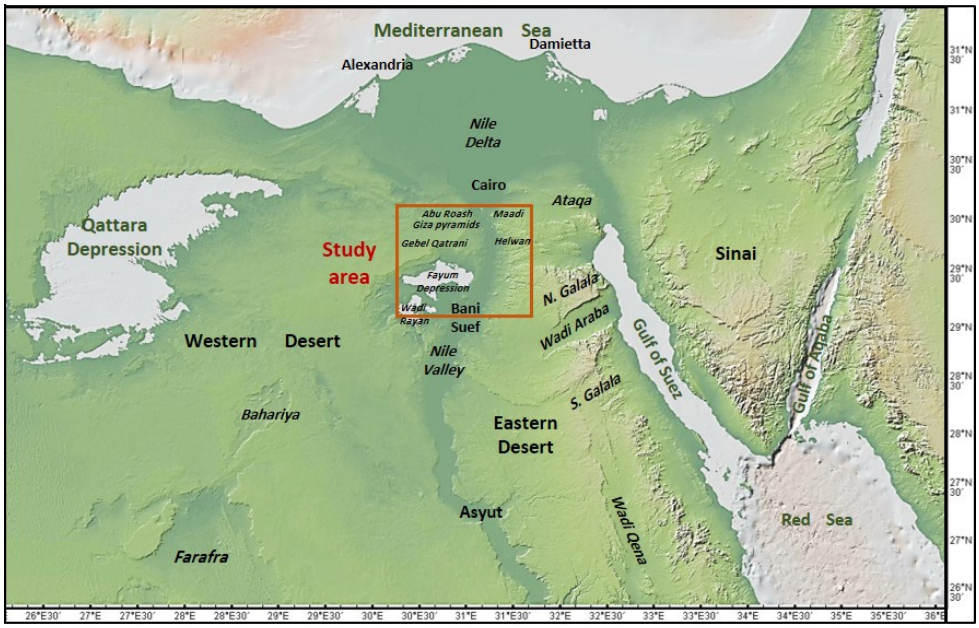

Fig. 1. Location of the study area.

exposed in Abu Roash area. These units were studied by Beadnell (1902), Fares (1948) and Jux (1954), they found these units belonging to the Cenomanian to Maastrichtian time interval. These units (about 398 m thick) found unconformably under the Paleocene and Middle Eocene carbonate units (Fig. 2). To the south, the Middle Eocene marl, shale and limestone units inside Fayum depression are capped unconformably by Oligocene clastic rocks that ended upward by at least two basaltic flows. Oligocene units are unconformably concealed under the Miocene dominantly sand unit.

On contrary, the Middle Eocene-Oligocene rock units are exposed in the eastern side of the study area (Fig. 2). The Middle Eocene carbonate units are juxtaposed against the Upper Eocene marl, shale, and impure limestone unit under the effects of faulting. This unit are capped unconformably by the Oligocene sand and gravel and then the Oligocene basaltic flows. The Miocene units are exposed further to the north of this side, at the both sides of the Cairo-Suez road.

In the Nile Valley and its desert fringes, the Pliocene-Quaternary sand and gravel filled the valley trough and its fluvial terraces, they extended to fill also El Fayum depression (Said, 1983).

The geologic ages are displayed in the following description instead of the rock units that could not be represented on the target geological map.

Upper Cretaceous units

Beadnell (1902), Faris (1948), and Jux (1954) published the first stratigraphic description and non-formal classification for the rock units building up the Abu Roash region. Based on the geologic age assigned for each Cretaceous rock unit, the present authors used the formal stratigraphic nomenclature for the whole Cretaceous units as designed in the subsurface Cretaceous hydrocarbon section.

The Turonian Sandstone Series is the oldest exposed Cretaceous unit in the Abu Roash region. It is equivalent Abu Roash "E" Member and is consisted of about 24 m thick of alternating thin-bedded sandstone, marl and shale that having greyish to green beds. Faris (1948) assigned the Cenomanian age to this unit, but it assigns here belonging to the Turonian age owing to the similarity of its lithologic and faunal assemblages as well as its stratigraphic position to those of the Turonian Abu Roash Member in subsurface.

Sandstone Series is conformably overlain by the Rudistae Series and Limestone Series, both series are equivalent to Abu Roash "D" Member (Turonian age by Faris (1948) and Said (1962)). The basal part of this member (Rudistae Series of the Cenomanian age as assigned by Jux (1954)) is composed of thin interbedded greyish to greenish yellow shale, marl, and limestone of about 30 m thick. While the upper part (Limestone Series) is made up of alternating limestone and dolomite beds (94 m thick).

Turonian Acteonella Series (Abu Roash "C" Member) rests conformably on the limestone Series. It is built up mainly of hard white limestone and chalky limestone beds with thin dolomitic limestone and marl interbeds (43 m thick). This limestone section is closely similar in color and lithology with the Turonian Flint Series (Abu Roash "B" Member), only the limestone beds of the Flint Series (47 m thick) have relatively thick beds rich in chert bands and nodules. The lower part of the Flint Series includes several green shales and yellowish-brown marl intercalation.

The Senonian rocks in Abu Roash region include the Plicatulla Series (Abu Roash "A" Member) and Chalk Series (Khoman Chalk). Plicatulla Series lies conformably on the Flint Series, the Plicatulla Series assigned as Coniacian-Santonian age (Faris, 1948) or Santonian age (Jux, 1954 and Said, 1962). The Plicatulla Series includes about 68 m of chalky beds at the base and yellowish limestone beds at the top.

In the northern and western parts of the Abu Roash region, the Plicatulla Series is unconformably overlain by lower part of Chalk Series (Campanian age by Faris, 1948 and Jux, 1954 or Campanian-Maastrichtian age by Said, 1962). This chalk unit has 78 m thick chalk to chalky limestones beds in Sudr El Khamis area where the chalk unit is unconformable overlain by the Middle Eocene rocks through a thin conglomerate bed (Moustafa, 1988).

Paleocene units

A thin Paleocene chalk and conglomerate section exists as a sandwich between the Chalk unit at the base and the Middle Eocene limestone at the top. The three units are separated by two unconformity surfaces (Haggag, 1986 and Strougo and Hottinger, 1987).

Middle-Upper Eocene units

Two sedimentary facies are observed during the deposition of the Middle-Upper Eocene rocks

in the study area. The carbonate and carbonate-clastic mixed facies are dominated during the deposition of the Middle and Upper Eocene units, respectively, on the eastern side of the study area whereas the carbonate-clastic mixed and clastic facies characterize the deposition of the Middle and Upper Eocene units around El Fayum area (south the western side of the study area).

The present study following the stratigraphic subdivision postulated by Strougo (1985a, b and 1986) and Strougo and Abd-Allah (1990) and its modification (Strougo, 2008) in the description of the Eocene units in the study area (Fig. 2).

Observatory Formation and Wadi Rayan Formation (Lutetian age)

The Observatory Formation is the oldest exposed complete rock unit in the eastern side of the study area. It consists of more than 87 m thick of hard limestones and chalky limestones with dolomitic ledges exist toward the top. These beds include several nummulitic horizons and rest conformably on the upper part of the Mokattam Formation (nummulitic limestone beds). The Mokattam Formation was assigned at Lutetian age whereas the Observatory

Formation at Lutetian/Bartonian age (Strougo, 1985a, b; Strougo and Abd-Allah, 1990; Strougo

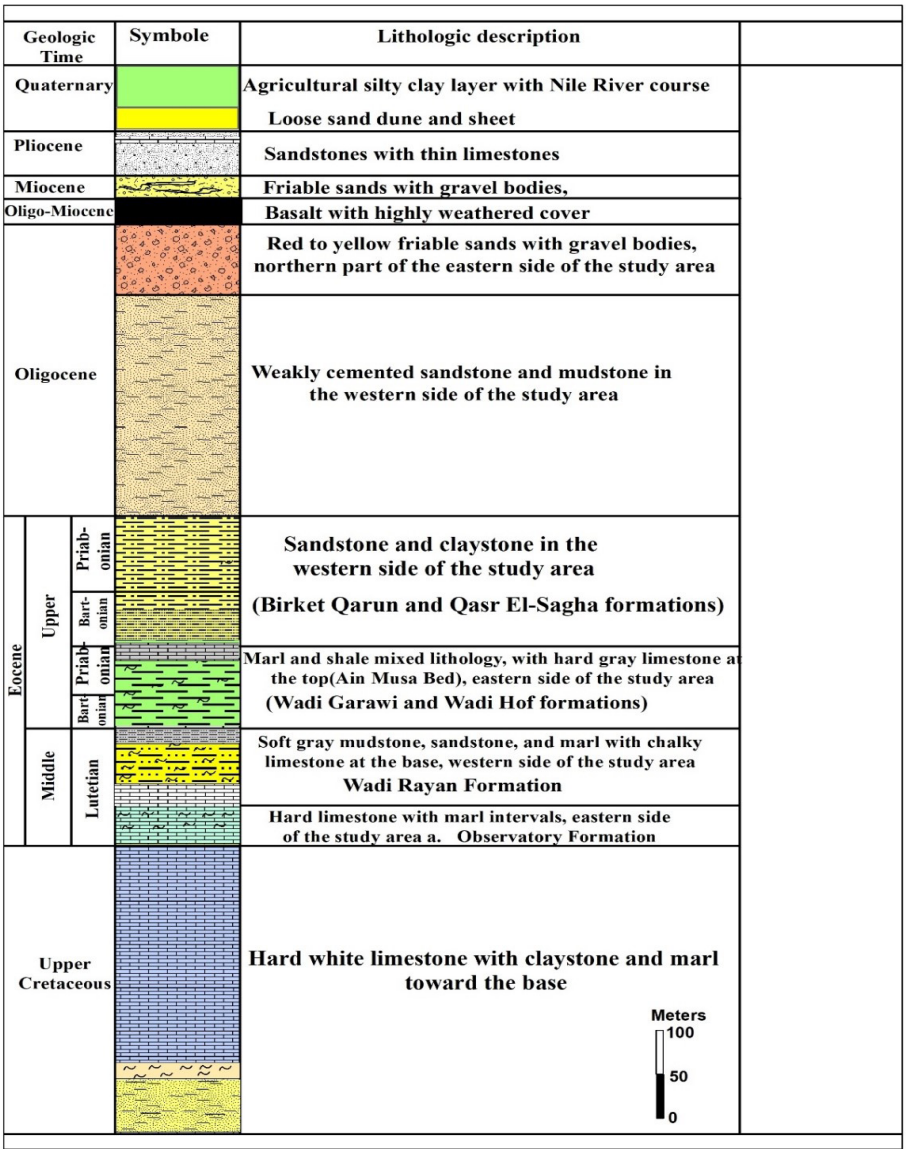

Fig. 2. General correlation of the stratigraphic units representing the exposed rocks in the eastern and western sides of the study area.

et al., 1992; and Strougo, 2008).

Wadi Rayan Formation (Said, 1962) or Wadi Rayan Group (Iskander, 1943) is the Lutetian-aged unit that is exposed in the western side of the study area (Fig. 2). According to Abu El Ghar (2012), the exposed lower part of this formation is consisted of snow white hard nummulitic limestone beds that coincide with the Samalut Formation and ends upward by an unconformity surface represented by about 50 cm of conglomerate layer. The middle part of Wadi Rayan Formation includes marl, claystone, and limestone intercalation (46 m thick, Muweilih Formation of Strougo, 2008) that graded upward into the nummulitic and bryozoan limestone and marl (63 m thick, Midawara Formation of Strougo, 2008) (Abdel-Fattah et al., 2010).

Qurn Formation and Gehannam Formation (Bartonian age)

The Qurn Formation in the study area consists mainly of marl and nummulitic chalky limestone at the base and relatively hard thin bedded limestone at the top (total thickness varies from 12 m to 38 m). The contact between the Observatory and Qurn Formations is sharp and characterized by an easily detectable small bench.

The Gehannam Formation is equivalent to the Qurn Formation in El Fayum area (Strougo, 2008). It is made up of dark gray mudstone with argillaceous limestone and calcareous sandstone beds (62 m thick).

Wadi Garawi and Wadi Hof formations and Birket Qarun and Qasr El-Sagha formations (Priabonian age)

According to Strougo (2008) the Wadi Garawi and Wadi Hof formations in both eastern side of the study area and Giza pyramids area are equivalent to the Birket Qarun and Qasr El-Sagha formations in El Fayum area (Fig. 2). The first two formations are built up mainly of greenish to grayish shales, yellowish marl, and sandy dolomitic limestone (total thickness is more than 55 m) whereas the last two formations include thick section of sandstone, claystone with mudstone interbeds that ends upward by white carbonate unit (total thickness is more than 85 m).

Oligocene sediments and basaltic flows

The Oligocene sediments (Gebel Qatrani Formation in the western side and Gebel Ahmeir Formation in the eastern side of the study area) are unconformably rest on the Upper Eocene rocks in the study area. These Oligocene sediments consist of loose to weakly cemented, varicolored sands and gravels (Fig. 2) with several sedimentary quartzites bodies and mudstone horizons. The thickness of these sediments is dramatically variable because they rest on a regional unconformity surface and are subjected to the weathering agents.

Egyptian Tertiary basalts were first described by Beadnell (1905) in the El Fayum area. At least three successive basalt sheets are observed in Wadan El-Faras, Gebel Qatrani by El Sheshtawi (1979) with a maximum thickness of 32 m and dated at early Oligocene, 31 Ma, by Meneissy and Abdelaal (1984). Basalt flows unconformably overly the Qatrani Formation and unconformably underlying the Miocene and/or Quaternary sediments. The Oligocene basaltic flows and Miocene units are exposed outside the limits of the eastern side of the study area.

Miocene unit

To the north of El Fayum depression in Gebel Qatrani, the Miocene sediments are exposed overlying the basaltic flows through an unconformity surface (Said, 1962). The Miocene Gebel Khashab formation consists mainly of sand and gravel body that have many mud intervals and petrified wood fragments.

Pliocene units

Pliocene rocks lie unconformably on the older rock units mainly in the eastern margin of Cairo-El Fayum road (Nile Valley bank) as well as those building up the desert fringes inside the Nile Valley. So, two completely different Pliocene facies are recognized in the study area. The first Pliocene facies fill the Nile Valley and includes mainly sand lithology that intercalated with dark claystone and gravel intervals (Kom El Shelul Formation). On contrary, the Pliocene facies on the Nile Valley bank that consist of sandstone with limestone interbeds.

This Kom El-Shelul Formation was introduced by Blankenhorn (1921) to describe the Early Pliocene sediments at area near the Giza Pyramids.

Quaternary sediments and agricultural clay

The Quaternary rock units includes two facies which are the aeolian sand and the agricultural clay layer inside the Nile Valley.

Aeolian sands cover large stretches of the El-Faiyum depression, especially around Qarun Lake and in the southwestern part of the area. In the

southwestern part, there are several longitudinal dunes with an NW-SE trend. The sand sheets cover a wide area around the Rayan Lake. These sand sheets extend northward to cover the vast areas lying at the both sides of the Cairo-El Fayum road.

The agricultural clay layer covers the major part inside the Nile Valley. It consists of more than 8m of dark gray silty clay.

Image Processing

The separation and/or discrimination of the lithologies constituting the exposed units and the affecting structures is the main target of the present study. These discriminations were followed by field checks and data measurements for each rock unit and each structural lineament. These done to construct detailed geologic maps for the study area and to define the most précised image characteristics that describing each lithology.

Data specifications

In the present study, the satellite images Landsat- 8 and Sentinel-2 were used and applied in the processing and enhancement of different algorithms and methods, such as Principal Component Analysis (PCA) and Independent Component Analysis (ICA).

Landsat- 8

Landsat- 8 satellite sensor (officially the Landsat Data Continuity Mission, LDCM) was dispatched on an Atlas-V rocket from Vandenberg Air Force Base, California on February 11, 2013. Multispectral imagery, Landsat 8 is downloaded from the USGS website (https://glovis.usgs.gov/). OLI and the TIRS are the main two sensors of Landsat 8 as shown in (Table 1). Four OLI scenes acquired in October 2019, were selected for the lithological discrimination. The VNIR and SWIR bands with 30 m spatial resolution of OLI were layer stacked and merged with the Panchromatic band of OLI and with 15 m spatial resolution to obtain a single file with 15m high spatial resolution image (Fig. 3).

Sentinel – 2

Sentinel-2A satellite sensor was effectively dispatched on June 23, 2015, at 03.51:58 am CEST from a Vega launcher structure the spaceport in Kourou, French Guiana. Sentinel-2A satellite is viewed as the main optical earth perception satellite in the European Copernicus program and was created and worked under the mechanical administration of Airbus Defense and Space for the European Space Agency (ESA). Sentinel-2A multispectral imagery was downloaded from the USGS website (https://glovis.usgs.gov/) and utilized in the present study. Specifications of spectral bands and resolution of Sentinel-2A is illustrated in (Table 2).

Four scenes acquired on 17 July 2021 were covered the area under investigation (T36RTU_20210717T082609,T36RTT_20210717t082609,T36RTU_20210715T083601, T36RUT_20210717T082609 and T36RTT_20210327T083601). After atmospheric correction by Actor module in ERDAS imagine software ver. 2014, for all the bands were layer

TABLE 1. Description of the operational land imager (OLI) sensor.

Band	Central Wavelength (µm)	Spatial Resolution (m)
Band1	0.4430	
Band2	0.4826	
Band3	0.5613	
Band4	0.6546	30
Band5	0.8646	
Band6	1.6090	
Band7	2.2010	
Band8	0.5917	15
Band9	1.3730	30
Band10	10.9000	100
Band11	12.0000	

TABLE 2. Specification of Sentinel-2A spectral bands.

Band No.	Central wavelength (µm)	Spatial Resolution (m)
Band 1- coastal aerosol	0.443	60
Band 2- blue	0.490	10
Band 3- Green	0.560	10
Band 4- Red	0.665	10
Band 5 – Vegetation Red Edge	0.705	20
Band 6 – Vegetation Red Edge	0.740	20
Band 7 – Vegetation Red Edge	0.783	20
Band 8 – NIR	0.842	10
Band 8a – Narrow NIR	0.865	20
Band 9 – water vapour	0.945	60
Band 10 – SWIR - Cirrus	1.375	60
Band 11 – SWIR	1.610	20
Band 12 – SWIR	2.190	20

stacked to one file with spatial resolution 10m (Fig. 4) except bands 1, 9, and 10 were prepared for atmospheric correction, they were removed from lithological classification in this study.

Image processing and lithological discrimination

Lithological discrimination is an analyzing imagery from one or more systems or sensors to identify different types of rock that can contribute to different types of geological mappings.

The present study is mainly depending on Landsat 8 and Sentinel-2 imagery in rock and structure discrimination. During the analysis, data was processed and mapped using remote sensing and GIS software. The most important methods of remote sensing techniques are PCA and ICA to achieve the present objects.

Principal Component Analysis

PCA is a technique for decreasing data redundancy by altering spectral values in photographs. Principal Component (PC) bands are the output of PCA transformation and are made up of bands that are not related to one another. PC1 has the data with the highest % variation, PC2 contains the data with the second highest percentage variance, and so on until the last PC that includes only the noise (Murti and Wicaksono 2014; Gasmi, et al., 2016).

The principal component analysis curtails the dimensionality of correlated optical multispectral datasets. It comprises the translocation of the origin and rotation of the data axes to better fit the brightness values of the input images (Corumluoglu et al. 2015). It was computed for Landsat 8 OLI data to evolve the best PCA for distinguishing the rock units in the study area. As the first three main components reflect the most variation, they have been allocated to show colors (Red (R), Green (G) and Blue (B)), respectively, to create the composite image of the PCA technique. From results (Table 3), PC1and PC2 shows strong absorption in band4, PC3 has strong absorptive in band 7, PC6 has strong absorptive in band 5 and high reflection in band, and PC7 shows strong absorptive in band 3 and high reflection in bands 1 and 5. Depending on the Eigen values extracted from PCA analysis, the first three principal components (PCI, PC2 and PC3) include more than 98% of all the information in Landsat images (Table 3).

Independent Component Analysis

Independent component analysis (ICA) is a statistical and computational technique for identifying hidden features in sets of random variables, measurements, or signals. It is considered as an extension to principal component and factor analysis. It is also, however, the more effective method able to identify the underlying variables or sources when the traditional methods fail entirely (Aapo et al., 2001). The main advantage of the ICA method over PCA is that it is dependent on the non-Gaussian assumption of independent sources, which is a significant component of hyperspectral datasets, (Veeramallu and Iyyanki, 2016). It discovers several intriguing characteristics in non-Gaussian hyperspectral images utilizing higher order statistics (Yusuf and He, 2011).

The first band in ICA has the highest eigenvalue, while the last band has the lowest

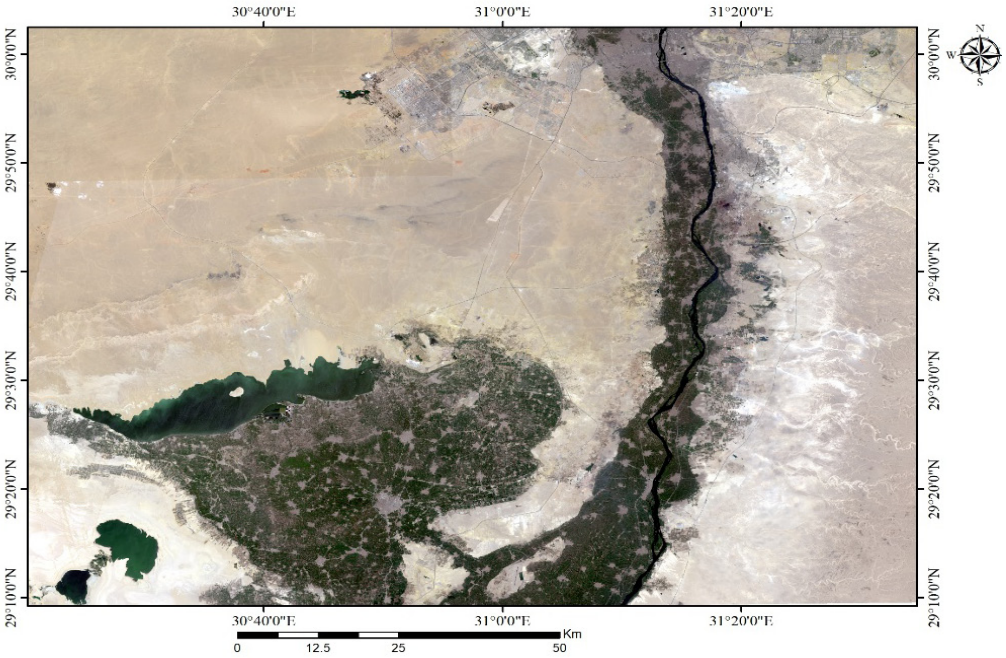

Fig. 3. True Color Composite of landsat-8 image (4,3,2 RGB) of the study area.

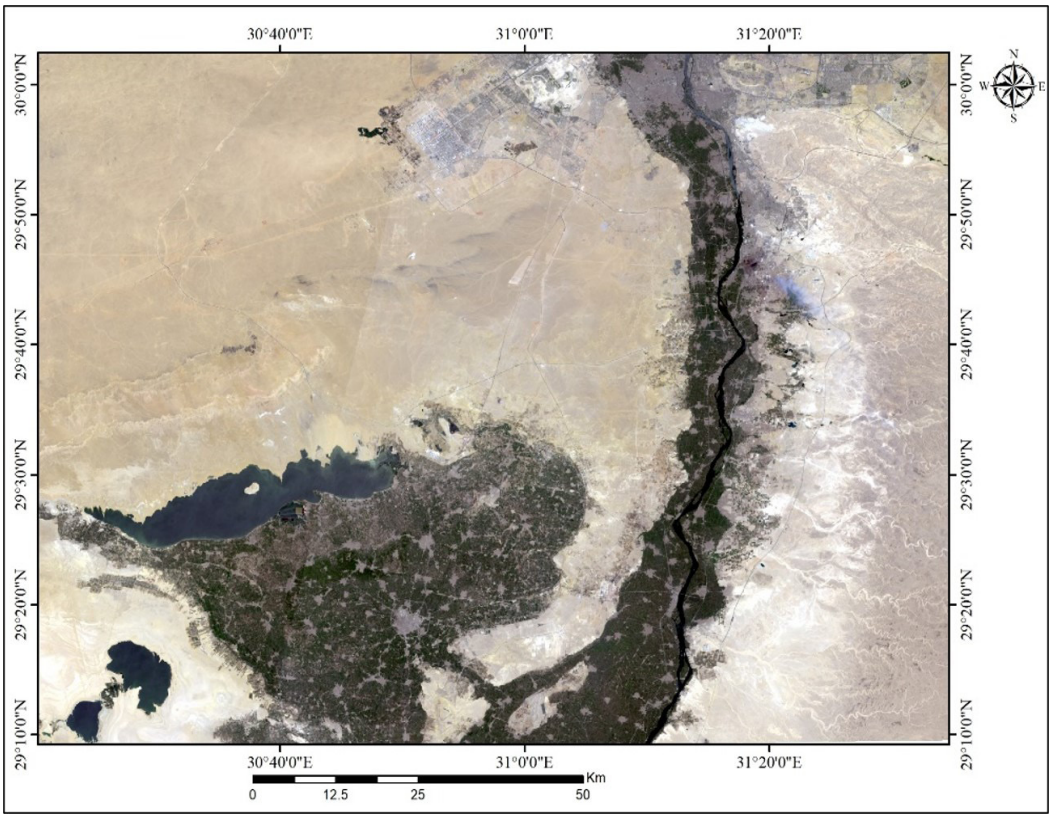

Fig. 4. True Color Composite of Sentinel-2A image (4,3,2 RGB) of the study area.

eigenvalue. The ICA method has been applied on sentinel-2A and landsat-8 satellite imagery in the present study and the results listed in table (4and 5). The results of ICA method of landsat-8 and Sentinel-2 data show the best band combination chosen for the identification the rock units in the study area, as in figures 7 and 8 respectively. The best five band combination of ICA of landsat-8 are (3 / 1 / 2, 6 / 2 / 3, 4 / 7 / 3, 6 / 7 / 4 and 6 / 5 / 3) RGB and six band combinations of ICA of Sentinel data ((3/ 11 / 5), (5/ 6 / 2), (7/ 2 / 11), (8a/ 5 / 2), (11 / 2 / 12) and (8a/ 11 / 12)) RGB. Eigen values extracted from ICA analysis of landsat-8 and Sentinel-2 are listed in tables 4 and 5 respectively, show the first three independent components (ICI, IC2 and IC3) include more than 98% and 95 % respectively of all information.

Results and Discussion

In the present study, the lithologic mapping of the study area is performed by integrated information resulting from PCS analysis of Landsat 8 image (PCA 1/5/4, PCA 3/1/2, PCA 4/3/2, PCA 4/7/3, PCA 6/5/3 RGB) and field observations and measurements.

TABLE 3. Eigenvector matrix and eigen value of the principal component analysis (PCA) of Landsat 8 OLI data.

Eigen Vector	PC1	PC2	PC3	PC4	PC5	PC6	PC7
B1	0.1143	-0.1147	0.3106	-0.5408	-0.0134	0.1365	0.1629
B2	0.1543	-0.1339	0.3585	-0.5648	-0.0304	0.1105	0.1974
B3	0.2639	-0.1373	0.3545	-0.0298	0.0272	-0.3008	-0.8329
B4	0.3970	-0.2368	0.2675	0.3395	-0.0763	-0.6004	0.4812
B5	0.3032	0.8972	0.2035	-0.0053	0.2363	-0.0476	0.0598
B6	0.5472	0.0991	-0.3415	-0.0515	-0.7315	0.1758	-0.0738
B7	0.5005	-0.2080	-0.5450	-0.1921	0.6098	-0.0203	-0.0050
Eigen value	146909747.9	5582307.7	3464118.2	326610.3	268826.4	193250.2	23634.4
Eigen value %	93.710	3.561	2.210	0.208	0.171	0.123	0.015

TABLE 4. Eigenvector matrix and eigen value of the Independent component analysis (ICA) of Landsat 8 OLI data.

Eigen Vector	IC1	IC2	IC3	IC4	IC5	IC6	IC7
B1	0.0006	0.0007	-0.0026	0.0010	0.0004	0.00002	0.00002
B2	-0.0003	-0.0003	0.0001	0.0003	-0.0001	-0.0004	0.0004
B3	0.0002	0.0002	0.0003	0.0000	-0.0001	0.0005	-0.0007
B4	-0.0008	-0.0010	0.0046	-0.0030	-0.0001	0.0002	0.0003
B5	0.0001	0.0002	0.0007	0.0009	0.0000	-0.0001	0.0000
B6	0.0010	0.0010	-0.0008	-0.0004	0.0002	-0.0006	0.0008
B7	0.0003	0.0002	0.0004	-0.0010	-0.0006	0.0012	-0.0005
Eigen value	11.29	0.43	0.43	0.09	0.06	0.05	0.008
Eigen value %	91.36	3.48	3.48	0.73	0.49	0.40	0.06

TABLE 5. Eigenvector matrix and eigen value of the Independent component analysis (ICA) of Sentinel-2 data.

Eigen Vector	IC2	IC3	IC4	IC5	IC6	IC7	IC8	IC8a	IC11	IC12
B2	0.006	-0.01	0.004	-0.002	0.003	-0.001	0.0007	0.0002	0.0004	0.00002
B3	0.004	-0.007	0.002	0.003	-0.006	0.003	0.0008	-0.0009	0.0002	-0.0001
B4	0.00008	0.001	-0.0009	-0.004	0.02	-0.01	-0.0003	0.001	0.001	-0.0009
B5	0.002	0.006	-0.004	-0.0002	-0.0007	0.001	-0.001	0.0005	0.001	-0.001
B6	0.004	-0.01	0.005	0.004	0.003	-0.001	0.001	0.0006	-0.005	0.0008
B7	-0.003	-0.0005	0.002	0.001	-0.0008	0.001	0.0005	-0.002	0.005	-0.006
B8	0.002	0.0008	-0.003	0.001	-0.0008	-0.001	0.007	-0.006	0.0007	0.00003
B8a	0.006	-0.007	-0.0008	-0.002	0.005	0.01	-0.0005	-0.01	0.002	-0.0004
B11	-0.009	0.01	-0.001	0.0002	-0.0009	0.0003	-0.00003	0.0009	-0.002	0.002
B12	0.002	-0.002	-0.008	0.01	-0.002	-0.002	0.001	0.001	-0.0006	0.0003
Eigen Value	19.4	4.6	2.3	0.85	0.24	0.16	0.09	0.06	0.02	0.013
%	69.95	16.59	8.29	3.06	0.87	0.58	0.32	0.22	0.07	0.05

The following are the lithological description for each rock unit exposed in the study area and the most representative remote sensing processing(s) that can be used in the separation of such lithologic composition in other areas. The resulted processing(s) are arranged from the most quality of separation (1st order to the least clearance 5th order, Table 6). The geologic interpretation of these remote sensing band combinations is discussed also.

lithologic and water body discriminations

Carbonate lithology

Two complete carbonate sections are exposed in the study area that are belonging to the Upper Cretaceous unit (UK) in Abu Roash area (Fig. 5a, c, d) and the Middle Eocene unit (m) that is exposed along the eastern side of the study area (Fig. 6 and Fig. 7a, c).

The Upper Cretaceous unit consists mainly of hard predominately white limestone, with thin marl and claystone interbeds toward its base (Fig. 6). This carbonate unit has small outcrop in the northeastern part of the Western Desert. The unit can be separated easily on the PCA images of processed Landsat 8 imagery data (PCAL) (PCA1/5/4RGB – PCA3/1/2RGB – PCA4/7/3RGB (Fig. 8 and Table 6), with a descending order of separation quality), it is interfered with the surrounding basalt and Oligocene sand on the PCA6/5/3RGB (Fig. 8). As, the separation of this carbonate unit on the ICA images of processed Landsat 8 imagery data (ICAL) has generally less quality, where it can be discriminated only on the ICA4/7/3RGB (Table 6), it is interfered with the surrounding

basalt and Oligocene sand on the other ICA images (Fig. 9). The separation quality of this unit increases on the ICA images resulted from the of processed Sentinel 2A imagery data (ICAS), the carbonate of this unit can be traced, with a descending order, from ICA8a/5/2RGB, ICA3/11/5RGB, ICA5/6/2RGB, ICA8a/11/12RGB, to ICA11/2/12RGB (Fig. 10 and Table 6). The unit is interfered with the surrounding sand and sandstone of the Oligocene and Miocene units on the ICA7/2/11RGB (Fig. 10).

On the other hand, the hard brownish yellow limestone beds with marl intervals of the Middle Eocene unit in the eastern side of the study area (m unit in Fig. 5) is separated roughly on the PCAL images PCA3/1/2RGB – PCA1/5/4RGB – PCA6/5/3RGB – PCA4/7/3RGB – PCA4/3/2RGB (Fig. 8 and Table 6), with a descending order. On these images, this carbonate unit building up Helwan plateau. the eastern part of this plateau is well discriminated on these images whereas its western slope side is badly defined owing to the dissecting wadis and building population. On all these images, there is a marked separation

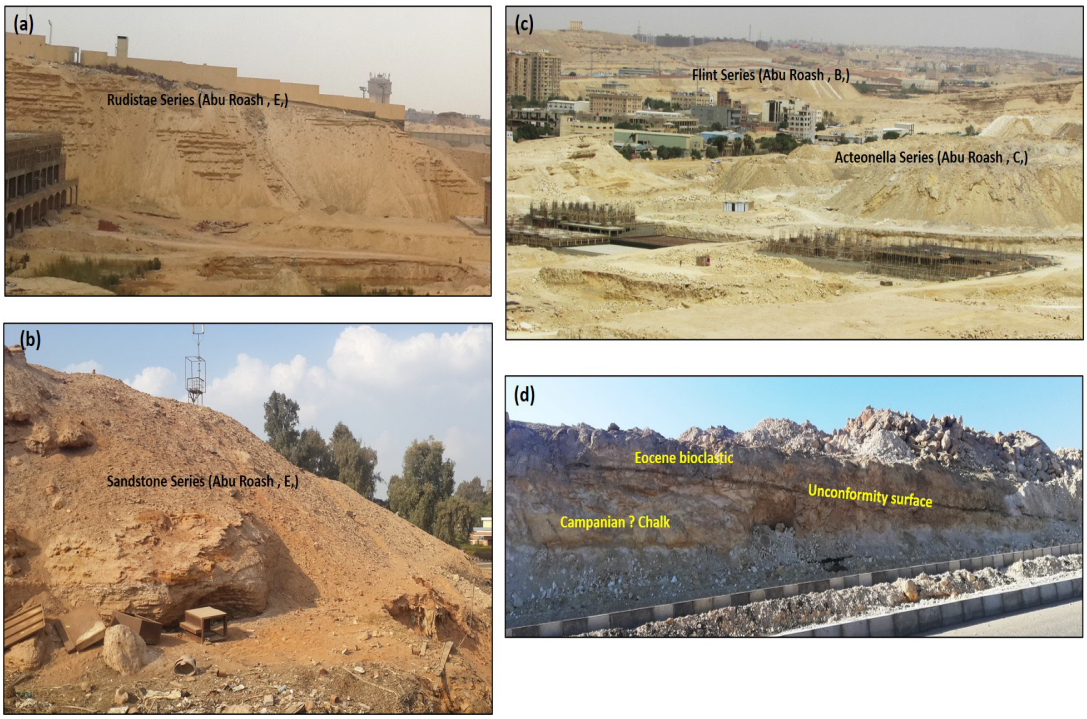

Fig. 5. Field photographs showing the Upper Cretaceous rock units in Abu Roash area.

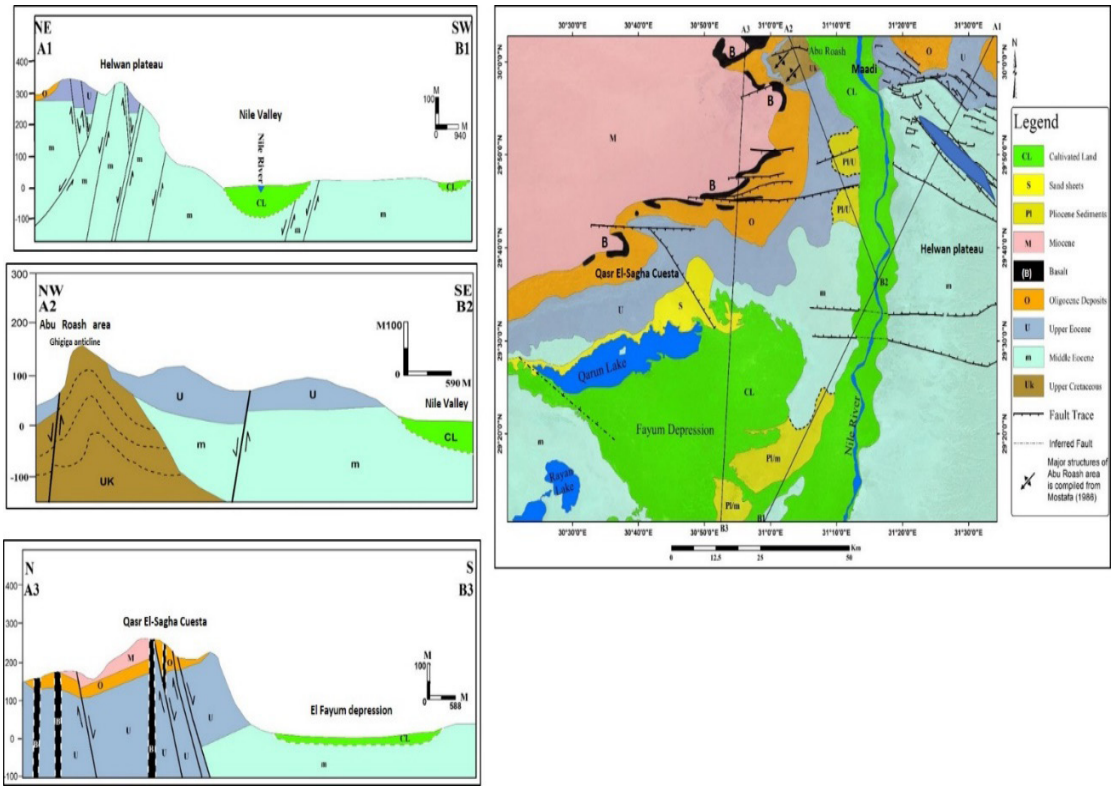

Fig. 6. Field geological map and three geologic cross sections in the study area.

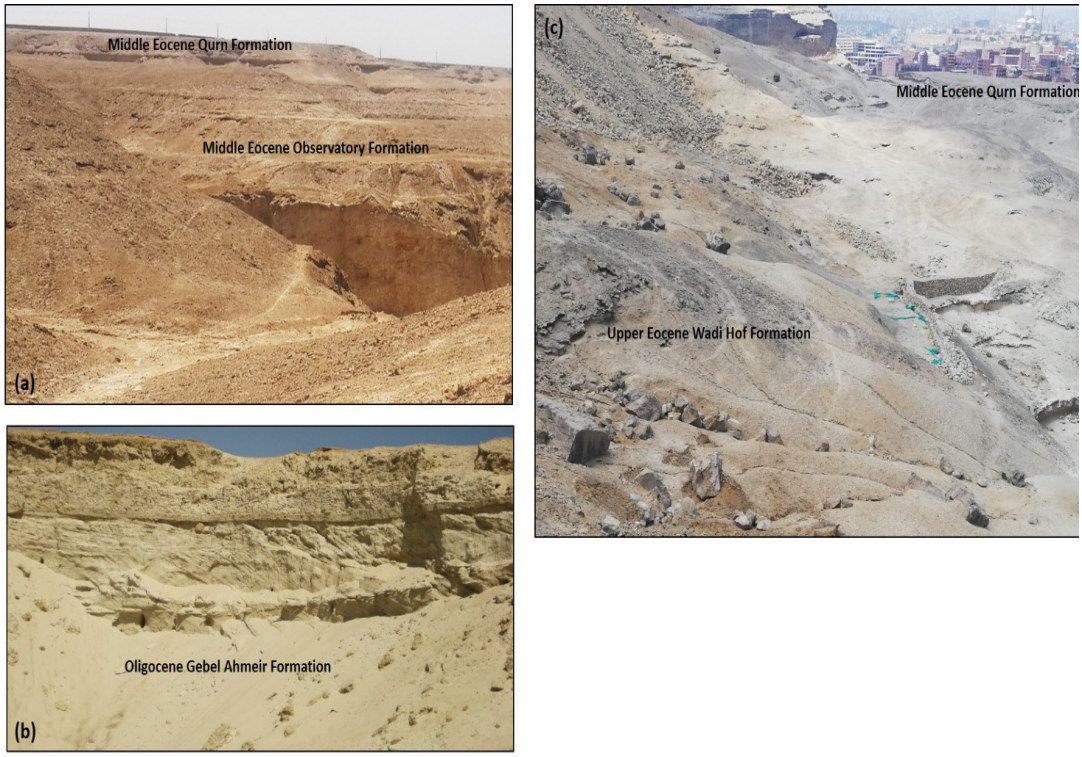

(Fig. 7): Field photographs showing the Middle-Upper Eocene rock units and the Oligocene sand unit that are exposed in the eastern side of the study area.

between the side slope and the sediments filling the Nile Valley. On contrary, the ICAs images fall in the separation of this carbonate unit. It can be separated roughly on ICA3/1/2RGB and ICA8a/5/2RGB, respectively, where the other images show strong interferences with the sediment filling the Nile Valley and the marl and shale of the Upper Eocene units (Figs. 9 and 10).

Marl and shale mixed lithology

The mixed marl and shale facies of the Upper Eocene unit is exposed in the eastern side of the study area (U unit in Fig. 5 and Fig. 7). These facies are capped by gray limestone (Ain Musa Bed). This unit is down faulted against the Middle Eocene hard limestone beds forming Helwan plateau and showing gentle dipping in some places.

The lithological heterogeneity made these mixed facies have different colors on the processed images (Figs. 8, 9, and 10). These facies are well expressed on the ICA images both processed Landsat 8 and Sentinel 2A imagery data (from Landsat 8 data: ICA6/2/3RGB – ICA6/7/4RGB – ICA4/7/3RGB – ICA6/5/3RGB - ICA3/1/2RGB, with a descending order; Fig. 9 and Table 6; from Sentinel 2A: ICA3/11/5RGB – ICA8a/5/2RGB – ICA8a/11/12RGB – ICA11/2/12RGB – ICA7/2/11RGB, with a descending order; Fig. 10 and Table 6). Good separation for this unit done on Landsat 8 data only on PCA4/7/3RGB and PCA3/1/2RGB images (Fig. 8 and Table 6).

Sandstone and claystone mixed lithology

The sandstone and claystone mixed facies are represented by the Upper Eocene units (Birket Qarun and Qasr El-Sagha formations) that exposed in the western side of the study area (U unit in Fig. 6 and Fig. 11). The Upper Eocene and Oligocene units show a northwestward gentle dipping that allowed the formation of Qasr El-Sagha cuesta in the areas just to the north of El Fayum depression (Fig. 6). The side slope of this cuesta is onlapped by the Miocene sand unit whereas it steep slope side is building up of the Upper Eocene and Oligocene units. the Upper Eocene unit is separated on the steep slope side by a bench-like topography (Fig. 6). This bench is observed in the field characterized the contact between the Upper Eocene Qasr El-Sagha Formation and the overlying Oligocene Gebel Qattrani Formation.

Like the previous marl and shale mixed facies, the Upper Eocene sandstone and claystone mixed facies are well represented on the ICA images rather than those on the PCA (Table 6). The PCAL images exhibit strong interferences with the overlying Oligocene sand (Fig. 8). On all the processed images (ICA and PCA), the upper contact of these mixed facies is defined easily by the bench topography (Figs. 8, 9, and 10). The sandstone and claystone mixed facies are well separated on the ICAs images, in a descending order of ICA7/2/11RGB - ICA8a/5/2RGB - ICA11/2/12RGB - ICA5/6/2 RGB. The other two images ICA8a/11/12RGB and ICA3/11/5RGB show strong interferences with the overlying Oligocene sand (Fig. 10 and Table 6). On the other hand, the ICAL images present less identification of these mixed facies on the ICA3/1/2RGB (some interference with the underlying Middle Eocene mudstone, sandstone, and marl unit) and ICA6/5/3RGB (with weak interference with the surrounding Oligocene sand, and Middle Eocene mudstone, sandstone, and marl) (Fig. 9 and Table 6).

Mudstone, sandstone, and marl mixed lithology

The Middle Eocene mixed mudstone, sandstone, and marl facies of the Wadi Rayan and Gehannam formations forming the eastern and western banks of El Fayum depression (Fig. 6). The two banks have nearly flat-topped surfaces, except the connected low areas that occupied by Wadi Rayan lakes in the western bank.

The lithological heterogeneity and nearly flat-topped surfaces made these mixed facies have different colors on most processed images (Figs. 8, 9, and 10). These facies are well represented by the ICAs images (from ICA8a/5/2RGB, ICA3/11/5RGB, ICA5/6/2RGB, ICA8a/11/12RGB, ICA11/2/12RGB, to ICA7/2/11RGB; with a descending order; Fig. 10 and Table 6) and by the PCAL images (from PCA1/5/4RGB, PCA3/1/2RGB, PCA4/3/2RGB, PCA6/5/3RGB, to PCA4/7/3RGB; with a descending order; Fig. 8 and Table 6). The separation of these mixed facies on the ICAL images done on ICA6/5/3RGB and ICA6/2/3RGB only (Fig. 9 and Table 6). Generally, the separation of these mixed facies in the western bank is better than that in the eastern bank owing to the recent sediments and weathering products covering the eastern one.

Friable to weakly cemented sand lithology

A predominate sand unit with some gravel bodies are exposed belonging to the Oligocene unit and Miocene unit at both sides of the study area (O unit and M unit in Figure 5 and Fig. 11). The Oligocene and Miocene units are involved within the Qasr El-Sagha cuesta (Figs. 6 and 11) whereas the Oligocene unit rest unconformably on the Upper Eocene marl and shale mixed facies in the low area that occupying the northern part

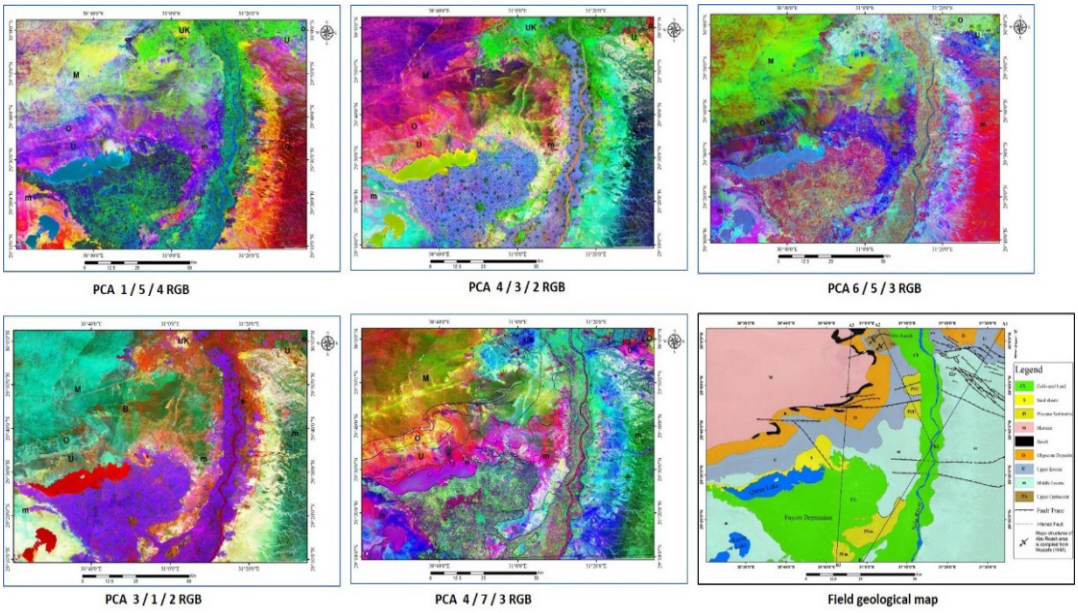

Fig. 8. Results of Principle component analysis (PCA) of Landsat-8 Imagery.

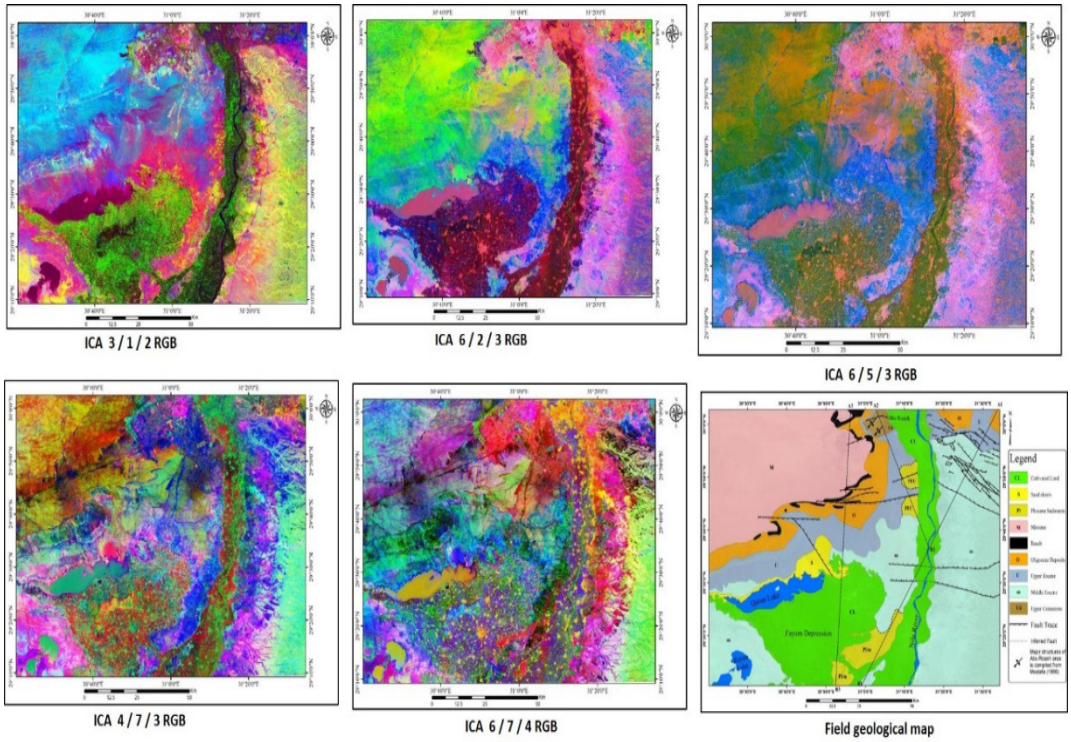

Fig. 9. Results of independent component analysis (ICA) of Landsat-8 Imagery.

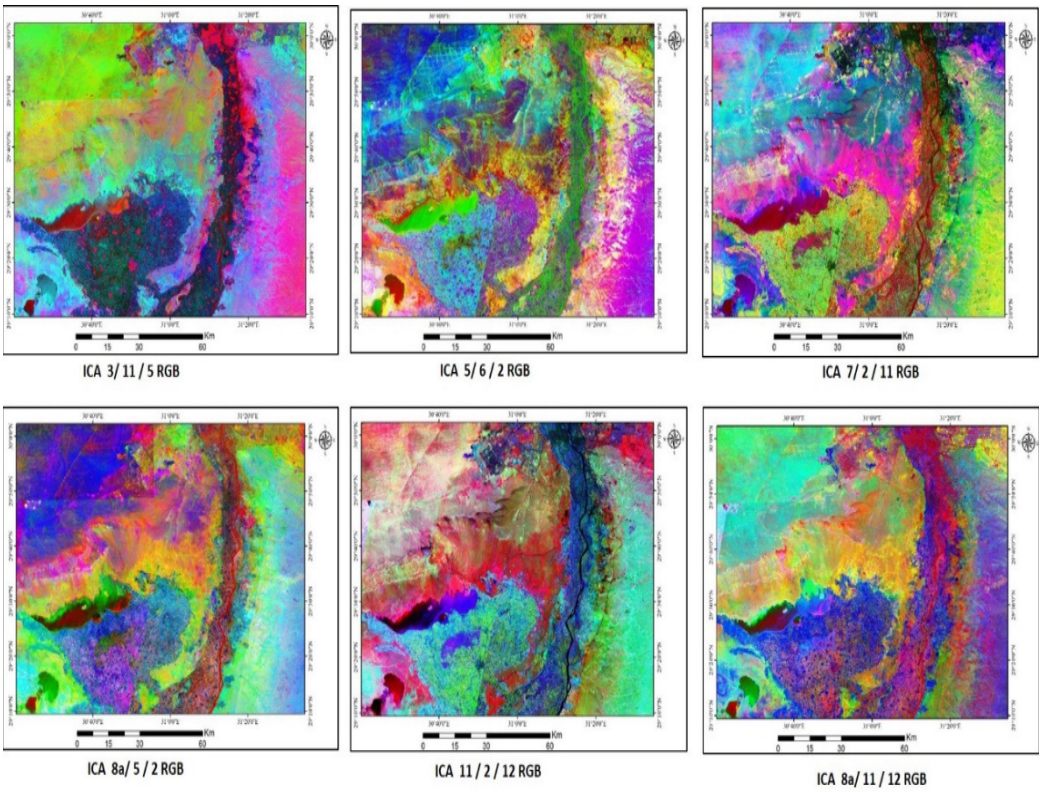

Fig. 10. Results of independent component analysis (ICA) of Sentinel-2A Imagery.

TABLE 6. Summary of the remote sensing processing of Landsat and Sentinel-2A data and the separation quality for each exposed lithologic unit.

Geologic time	Lithologic description		PCA Band Discrimination (RGB) / ICA Band Discrimination (RGB)				
		Imagery data	1st order	2nd order	3rd order	4th order	5th order
Recent	Water bodies	Qarun lake	Landsat 8	PCA3/1/2	PCA4/3/2	PCA1/5/4	PCA4/7/3	PCA6/5/3
				ICA6/7/4	ICA4/7/3	ICA6/2/3	ICA3/1/2	ICA6/5/3
			Sentinel-2A	ICA5/6/2	ICA11/2/12	ICA7/2/11	Incomplete lake boundaries	
		Wadi Rayan lakes	Landsat 8	PCA3/1/2	PCA1/5/4	No sharp contacts with the surrounding lands		
				ICA3/1/2	ICA6/2/3	ICA6/7/4	ICA4/7/3	
			Sentinel-2A	ICA5/6/2	ICA11/2/12	ICA8a/11/12	ICA8a/5/2	ICA3/11/5
Quaternary	Agricultural silty clay layer with Nile River course, (CL unit, Fig. 6)		Landsat 8	PCA4/7/3	PCA4/3/2	PCA6/5/3	PCA1/5/4	PCA3/1/2
				ICA3/1/2	ICA6/5/3	ICA6/2/3	ICA4/7/3	ICA6/7/4
			Sentinel-2A	ICA3/11/5	ICA5/6/2	ICA11/2/12	ICA8a/5/2	ICA8a/11/12
	Loose sand dune and sheet, (S unit, Fig. 6)		Landsat 8	PCA3/1/2	PCA1/5/4	PCA6/5/3	ICA11/2/12	
				ICA6/2/3	ICA4/7/3	ICA6/7/4	ICA3/1/2	
			Sentinel-2A	ICA8a/11/12	ICA8a/5/2	ICA3/11/5	ICA1/2/12	
Pliocene	Sandstones with thin limestones, (PI unit, Fig. 6)		Landsat 8	Is badly expressed on the images owing to its sandstone similarity with the surrounding Upper Eocene sandstone.				
			Sentinel-2A	ICA3/11/5	ICA8a/11/12	Badly expressed on the other images		
Miocene	Friable sands with gravel bodies, (M unit, Fig. 6).		Landsat 8	PCA6/5/3	PCA1/5/4	PCA4/7/3	Interference with the Upper Eocene and Oligocene units	
				ICA3/1/2	ICA6/5/3	ICA4/7/3		
			Sentinel-2A	ICA8a/11/12	ICA7/2/11	ICA8a/5/2	ICA11/2/12	ICA5/6/2
Oligo-Miocene	Basalt with highly weathered cover, (Black colored unit, Fig. 6).		Landsat 8	PCA3/1/2	PCA6/5/3	Strong interference with the surrounding units		
				ICA4/7/3	ICA3/1/2	ICA6/7/4	Strong interference	
			Sentinel-2A	ICA11/2/12	ICA8a/11/12	ICA7/2/11	ICA3/11/5	
Oligocene	Red to yellow friable sands with gravel bodies, northern part of the eastern side of the study area (O unit, Fig. 6).		Landsat 8	PCA3/1/2	PCA4/7/3	Interference with the Upper Eocene sandstone		
			Sentinel-2A	ICA3/1/2	ICA6/2/3	ICA6/7/4	ICA4/7/3	ICA6/5/3
				ICA8a/5/2	ICA8a/11/12	ICA3/11/5	ICA5/6/2	ICA11/2/12
	Weakly cemented sandstone and mudstone in the western side of the study area, (O unit, Fig. 6).		Landsat 8	PCA1/5/4	PCA3/1/2	PCA4/7/3	PCA4/3/2	PCA6/5/3
			Sentinel-2A	ICA3/1/2	ICA4/7/3	ICA6/7/4	ICA6/5/3	ICA6/2/3
				ICA8a/11/12	ICA8a/5/2	ICA7/2/11	ICA5/6/2	ICA11/2/12
Eocene / Upper	Marl and shale mixed lithology, with hard gray limestone at the top (Ain Musa Bed), eastern side of the study area (U unit, Fig. 6).		Landsat 8	PCA4/7/3	PCA3/1/2	Interfered with the sand and limestone units		
				ICA6/2/3	ICA6/7/4	ICA4/7/3	ICA6/5/3	ICA3/1/2
			Sentinel-2A	ICA3/11/5	ICA8a/5/2	ICA8a/11/12	ICA11/2/12	ICA7/2/11
	Sandstone and claystone in the western side of the study area, (U unit, Fig. 6).		Landsat 8	PCA images show strong interferences with the overlying Oligocene sand.				
				ICA3/1/2	ICA6/5/3	Interfered with the overlying Oligocene sand.		
			Sentinel-2A	ICA7/2/11	ICA8a/5/2	ICA11/2/12	ICA5/6/2	
Middle	Hard limestone with marl intervals, eastern side of the study area (m unit, Fig. 6).		Landsat 8	PCA3/1/2	PCA1/5/4	PCA6/5/3	PCA4/7/3	PCA4/3/2
				ICA3/1/2	Strong interference with the Nile sediments, marl, and shale			
			Sentinel-2A	ICA8a/5/2	Strong interference with the Nile sediments			
	Soft gray mudstone, sandstone, and marl with chalky limestone at the base, western side of the study area (m unit, Fig. 6).		Landsat 8	PCA1/5/4	PCA3/1/2	PCA4/3/2	PCA6/5/3	PCA4/7/3
				ICA6/5/3	ICA6/2/3	Interferences with other units and multicolor		
			Sentinel-2A	ICA8a/5/2	ICA3/11/5	ICA5/6/2	ICA8a/11/12	ICA11/2/12
Upper Cretaceous	Hard white limestone with claystone and marl toward the base, (UK unit, Fig. 6).		Landsat 8	PCA1/5/4	PCA3/1/2	PCA4/3/2	PCA4/7/3	
				ICA4/7/3	ICA3/1/2	Interfered with the basalt and sand units		
			Sentinel-2A	ICA8a/5/2	ICA3/11/5	ICA5/6/2	ICA8a/11/12	ICA11/2/12

Note that: the 1st order is referring to the highest quality of separation whereas the 5th order referring to the lowest quality.

Fig. 11. Field photographs showing the Upper Eocene-Oligocene rock units forming Qasr El-Sagha cuesta to the north of El Fayum depression.

of the eastern side of the study area. Also, the Oligocene sediments in the eastern side exist as very thick bedded friable sand whereas the Oligocene sand have relatively thin bedded and weakly cemented sand with mudstone and gravel interbeds in the western side of the study area.

The Oligocene friable sand have relatively small outcrops in the eastern side of the study area. This sand unit is easily separated better on both ICAs images than the ICAL and PCAL images. The ICAs images show a descending order of separation quality from ICA8a/5/2RGB, ICA8a/11/12RGB, ICA3/11/5RGB, ICA5/ 6/2RGB to ICA11/2/12RGB

(Fig. 10 and Table 6). The unit is interfered with the Upper Eocene mixed marl and shale facies on the ICA7/2/11RGB. On the other hand, the ICAL images have separation quality from ICA3/1/3RGB, ICA6/2/3RGB, ICA6/7/4RGB, ICA4/7/3RGB to ICA6/5/3RGB (Fig. 9 and Table 6). The unit is traced only on the PCA3/1/2RGB and PCA4/7/3RGB of Landsat imagery data and found interfered with the surrounding Upper Eocene marl and shale mixed facies on the other PCA images (Fig. 8 and Table 6).

The weakly cemented sand of the Oligocene unit and the Miocene friable sand are strongly interfered on most processed images covering the western side of the study area owing to their lithologic and petrological similarities (Figs. 8, 9, and 10). The ICAs images exhibit strong interference between the Oligocene sand and Miocene sand (Fig. 9) whereas the PCAL images show strong interference between the Oligocene sand and Upper Eocene sandstone and mudstone mixed facies (Fig. 8). As the ICAs images reveal generally incomplete outcrops of the Oligocene unit with interference with the Upper Eocene unit (Fig. 10).

The friable sand body of the Miocene unit covering the northwestern part of the study area (M unit in Fig. 5) has mostly on the processed images more than one color (Figs. 8, 9, and 11). The Miocene sand unit is represented by strongly when it has single color on PCAL image (green color on 6/5/3RGB), ICAL image (pale yellow color on 3/1/2RGB), and ICAs image (pale yellow color on 8a/11/12RGB) (Table 6). The unit has multicolor on other processed images and show strong interference with the Oligocene and Upper Eocene sand and sandstone, respectively (Figs. 8, 9, and 10).

Basaltic flows

Highly weathered basaltic flows are exposed as thin sandwiches between the Oligocene and Miocene units in the western side of the study area (B unit in Fig. 6 and Fig. 11). The thickness of these flows controlled the separation quality on the images. The whole basaltic flows in the study area are discriminated well on most images whereas the large (thick) flow parts are separated only on the PCAL (6/5/3RGB) and ICAs (7/2/11RGB). Generally, the ICA technique of both Landsat and Sentinel 2A imagery data show good separation quality than that shown by the PCAL technique (Table 6).

Silty agricultural clay layer

The Holocene agricultural silty clay layer occupies the central strip of the Nile Valley (CL unit in Fig. 6). The traditional agricultural activity and related channel and drainage system as well as the Nile River and buildings rest on the top of this flat-lying layer. The outcrops of this layer are bounded from the east and west by desert fringes that are built up mainly of the Pliocene-

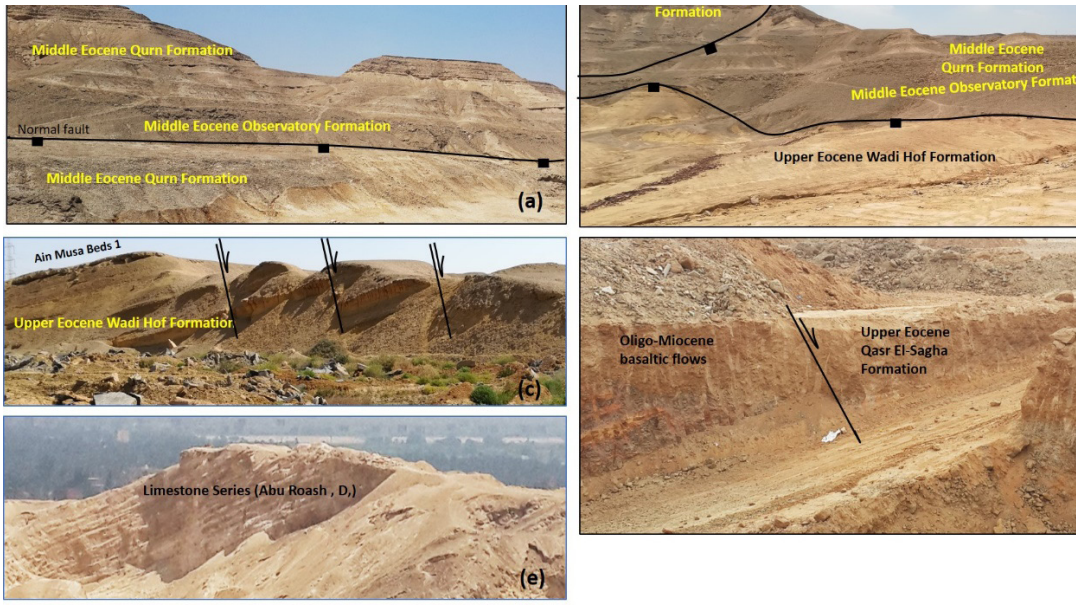

Fig. 12. Field photographs showing the structures affecting the Middle Eocene units in the eastern side (a), the Middle-Upper Eocene rock units in the eastern side (b), the Upper Eocene Wadi Hof Formation in the eastern side (c), the basaltic flows in the western side (d), the limb of Ghigaga anticline in the western side (e).

Pleistocene sand, gravel, and clay.

The discrimination of this silty clay layer and its top-lying features on the present processed images depends on the layer boundaries with the desert fringes, Nile River and irrigation and drainage systems, and buildings. On using the present two imagery data, the PCA images show separation quality better than the ICA images (Figs. 8, 9, 10). Generally, these images have different qualities on the separation of this layer boundaries and its top-lying features. The separation quality of the Holocene silty clay layer on the PCAL images is PCA4/7/3RGB (showing outcrops, irrigation system, Nile River, and buildings), PCA4/3/2RGB (showing buildings), PCA6/5/3RGB (showing buildings), PCA1/5/4RGB, and PCA3/1/2RGB; with a descending order (Fig. 8 and Table 6). The tracing of this layer on the ICAL images has the ICA3/1/2RGB - ICA6/5/3RGB - ICA6/2/3RGB - ICA4/7/3RGB - ICA6/7/4RGB quality sequence (Fig. 9 and Table 6). As the separation of the layer on the ICAs images follows the ICA3/11/5RGB (showing outcrops and agricultures) – ICA5/6/2RGB (showing outcrops and Nile River) - ICA11/2/12RGB (showing Nile River and irrigation system) - ICA8/5/2RGB – ICA8a/11/12RGB sequence (Fig. 10 and Table 6).

Sandstone with thin limestone interbeds

The Pliocene sandstone with thin limestone intercalation unit (PI unit in Fig. 6) is badly expressed on the processed images owing to thin outcrop section and its lithologic similarity with the surrounding Upper Eocene sandstone unit. The Pliocene unit is roughly observed only on the ICA3/11/5RGB and ICA8a/11/12RGB images of Sentinel imagery data (Fig. 10 and Table 6).

Sand dunes and sheets

Loose sand dunes and sheets (S unit in Fig. 6) can be traced on the processed image depending on its outcrop width. This unit exists having a wide outcrop lying to the northeast of the Qarun lake and a narrow outcrop occupying the northern strip of this lake. The wide sand outcrop is presented on all Landsat images whereas the narrow one is expressed only by the PCA3/1/2RGB, ICA6/2/3RGB and ICA4/7/3RGB (Figs. 8 and 9, Table 6). On contrary, both wide and narrow sand outcrops are well discriminated on the ICAs images having the ICA8a/11/12RGB - ICA8a/5/2RGB - ICA3/11/5RGB – ICA11/2/12RGB quality sequence (Fig. 10 and Table 6).

Qarun lake and Wadi Rayan lakes

Two large water bodies exist in El Fayum area, which are Qarun lake and Wadi Rayan lakes. The separation of these two bodies on the processed images depended on the sharpness of the water contact with the land and the horizontal extension of the water body.

The northern part of El Fayum depression is occupied by the Qarun lake which is considered by Marks et al. (2018) as relic of the early-middle Holocene freshwater reservoir. They are indicated also that the maximum depth of the Qarun lake is about 8.5 m (-55 m below sea level) and its highly saline water filling attain more than 30,000 ppm.

As Wadi Rayan lakes on the western bank of El Fayum depression includes two large lakes. The northern lake (upper lake) is connected to the southern lake (lower lake) by a water channel that runs through cascading ground terraces and ends southward by a conspicuous water fall feature before reaching the southern lake. The two lakes have relatively lower water salinity than that measured in the Qarun lake, the upper lake has water salinity varying between 1400 and 1500 ppm whereas the lower lake has 4500 to 6100 ppm (water salinity data from Hereher, 2015). The maximum depth of the upper lake is – 21 m below sea level whereas it's for the lower lake is -59 m below sea level (El Diftar, 1983).

The separation of the Qarun and Wadi Rayan lakes on the present images strongly show variation in the separation quality. These include the incomplete outcrop patterns and the sharpness of their contacts with the lands, but in all images the water in these lakes do not show any interference with the surrounding lands (Figs. 8, 9, and 10).

The possessed PCAL and ICAL images show better separation quality for the Qarun lake than those done using the Sentinel 2A imagery data. The good separation quality of this lake on the PCAL images is PCA4/3/2RGB, PCA3/1/2RGB, PCA1/5/4RGB, PCA4/7/3RGB, and PCA6/5/3RGB, with a descending order (Fig. 8 and Table 6). On the other hand, the separation quality on the ICAL images is ICA6/7/4RGB, ICA4/7/3RGB, ICA6/2/3RGB, ICA3/1/2RGB and ICA6/5/3RGB, with a descending order (Fig. 9 and Table 6). The least separation quality of this lake was on the ICAs images (ICA5/6/2RGB, ICA11/2/12RGB, and ICA7/2/11RGB, with a descending order Fig. 10 and Table 6), the other

ICAs images show incomplete outcrop pattern for the lake (Fig. 10).

On contrary, the separation quality of the Wadi Rayan lakes on possessed images using the ICAs images is better than the images resulted from the PCAL and ICAL techniques. The separation quality of the Qarun lake on the ICAs images is ICA5/6/2RGB, ICA11/2/12RGB, ICA8a/11/12RGB, ICA8a/5/2RGB and ICA3/11/5RGB, with a descending order (Fig. 10 and Table 6). These images are the only ones that showing the differences in the ground and levels and in water levels inside the two lakes of Wadi Rayan (Fig. 10). Wadi Rayan lakes are discriminated on four ICAL images (ICA3/1/2RGB, ICA6/2/3RGB, ICA6/7/4RGB, and ICA4/7/3RGB; with a descending order; Fig. 9 and Table 6). The two lakes are classified on only two PCAL images (PCA3/1/2RGB and PCA1/5/4RGB) whereas the other images show weak contact sharpness (Fig. 8 and Table 6).

Affecting structures

The processed images of Landsat and Sentinel 2A imagery data show only the northwest oriented faults affecting Helwan plateau, east-west trending faults that offset the basaltic sheets (north El Fayum), and the northwest-dipping of Qasr El-Sagha cuesta. The highly deformed Upper Cretaceous rocks in Abu Roash area are hardly recognized on the present images scale.

Qasr El-Sagha cuesta and its slope (dipping) side and scarp side are clearly recognized on all processed images with different separation quality. The bench topography that separated the Upper Eocene unit from the Middle Eocene unit in the scarp side is traced as well.

The northwest striking faults affecting the northern part of Helwan plateau are traced with reasonable quality on the ICAL6/7/4RGB and ICAs5/6/2RGB (Fig. 9).

The east-west faults that offseted the basaltic sheets are clearly mapped on the PCAL3/1/2RGB, ICAL3/1/2RGB, and ICAL4/7/3 images, as well as they are mapped on the ICAs11/2/12RGB and ICAs3/11/5RGB (Figs 9 and 10).

The mapping of the affecting structures in the study area (Fig. 6) depended mainly on the field observations and measurements rather than the structural separation of the processed images.

Geologic interpretation of the band combinations

The lithologies discriminated in the study area are classified into single (pure) facies and mixed facies, depending on the lithologic composition and intercalations. Owing to the outcrop area, lithologic unit thickness, and lithologic homogeneity, these facies are hard limestone (Middle Eocene, east side), limestone mixed with marl; shale; and sandstone (Upper Cretaceous, Abu Roash), limestone mixed with shale and marl (Upper Eocene, east side), friable to weakly cemented sand (Miocene, west side and Oligocene east side), loose sand dune and sheets, sandstone and mudstone (Oligocene, west side), sandstone and claystone (Oligocene west side), mudstone; marl; and sandstone (Middle Eocene, west side), Nile Valley agricultural systems, and Qarun and Wadi Rayan lakes.

The hard grayish yellow to white limestone with marl interbeds forming Helwan plateau in the eastern side of the study area (Fig. 6) are represented well by PCAL3/1/2RGB, ICAL3/1/2RGB, and ICAs8a/5/2RGB images (Figs. 8, 9 and 10). When mixing predominate limestone beds with marl, shale, and sandstone beds, as in Abu Roash area, the separation quality on the PCAL3/1/2RGB and ICAL3/1/2RGB images decreases whereas the quality on the ICAs8a/5/2RGB image still clear (Fig. 10) Also, the quality separation on both PCAL1/4/5RGB image (second order in pure limestone) and ICAL4/7/3RGB image increases. As the marl, limestone, and shale mixed facies of the Upper Eocene unit in the eastern side are well represented on the PCAL4/7/3RGB, ICAL6/2/3RGB, and ICAs3/11/5RGB images. The quality separation of these mixed facies on the PCAL3/1/2RGB and ICAL3/1/2RGB decreases (Figs. 8, 9 and 10).

On considering the clastic sand size on the processed images, we differentiate first between the friable to weakly cemented sand, loose sand dunes and sheets, and sandstone lithologies. The friable to weakly cemented sand of the Miocene unit in the western side (Fig. 6) are well demonstrated on the PCAL6/5/3RGB, ICAL3/1/2RGB, and ICAs8a/11/12RGB images, whereas the friable to weakly cemented sand of the Oligocene unit in the eastern side are exhibited well on the PCAL3/1/2RGB, ICAL3/1/2RGB, and ICAs8a/5/2RGB images (Figs. 8, 9 and 10). The ICAL3/1/2RGB images show well these two friable sand units. While the PCAL6/5/3RGB and ICAs8a/11/12RGB images of the Miocene

unit are replaced by the PCAL3/1/2RGB and ICAs8a/5/2RGB images, respectively. These changes in band combination are suggested to the red coloration (ferruginous oxides) and dark lag gravels surface covering the Oligocene unit. The more compacted and cemented sandstone and mudstone of the Oligocene unit in the west of the study area (Fig. 6) is well expressed on the PCAL1/5/4RGB, ICAL3/1/2RGB, and ICAs8a/11/12RGB images (Figs. 8, 9 and 10). The mudstone mixing and rock compaction and cementation made little changes in the band combinations of the clastic sand size. The ICAL6/3/2RGB ratio can be used to differentiate the sand dunes and sheets unit from the other sand size lithologies (Fig. 9). The other high-quality separations of this unit are on the PCA_L3/1/2RGB and ICAs8a/11/12RGB ratios (Figs. 8, 9 and10). The ICAL3/1/2RGB characterizes the separation of the other three sand size units in the study area whereas the other 8 band ratios arranged having separation quality between first and second orders (Fig. 12b).

The sandstone, claystone, and mudstone mixed facies of the Upper Eocene unit in the western side (Fig. 6) is well separated on the ICAL3/1/2RGB and ICAs7/2/11RGB images (Figs. 8, 9 and 10), where the PCAL images show strong interference with the surrounding clastic units. The introducing of marl to these mixed facies (as found in the Middle Eocene unit in the western side) changed completely the discrimination of the Middle Eocene unit on the processed images. This unit are well discriminated on the PCAL1/5/4RGB, ICAL6/5/3RGB, and ICAs8a/5/2RGB images (Figs. 8, 9 and 10). The ICAs8a/5/2RGB ratio also characterizes the separation of the pure limestone.

Large water bodies exist in the study area as Qarun lake and Wadi Rayan lakes. The Qarun lake is well demonstrated on the PCAL3/1/2RGB, ICAL6/7/4RGB, and ICAs5/6/2RGB images (Figs. 8, 9 and 10). While the Wadi Rayan lakes are traced well on the 3/1/2RGB ratio of both PCAL and ICAL (Figs. 8, 9 and 10) as well as the 6 (Fig. 10). All ICAs images illustrate well the ground elevation differences exist between the deepest points for the study three lakes, where the deepest portions of the Qarun lake (- 55 m below sea level) and lower Wadi Rayan lake (-59 m below sea level) have the same image colors and are separated from the shallow deepest portion of the upper wadi Rayan lake (has different color) on all ICAs images (Fig. 10). In addition to this ground elevation difference, the water salinity could be played the second factor which controlled the changes in these band combinations that exist between the Qarun lake (about 30,000 ppm) and Wadi Rayan lakes (1, 400 to 6,100 ppm). On contrary, the small water body of the Nile River is well illustrated with good quality only by ICAs11/2/12RGB and ICAs3/11/5RGB ratios (Fig. 10).

Less water saturation is recorded through the agricultural layer and related systems in the Nile Valley. These systems include the water system (channel and drain network), agricultural cover system, and building systems. The water system is well shown on the PCAL4/7/3RGB, ICAs5/6/2RGB, and ICAs11/2/12RGB images, whereas the agricultural system on the ICA3/11/5RGB image. The buildings are separated well on the PCA4/7/3RGB, PCA4/3/2RGB, PCA6/5/3RGB, and PCA1/5/4RGB images. Generally, the agricultural layer and its systems are well traced on the PCAL4/7/3RGB, ICAL3/1/2RGB, and ICAs3/11/5RGB images (Figs. 8, 9 and 10), The complex systems covering the agricultural layer made us hardly differentiating its characteristic ratios from those describing the other remote sensing units.

Several geologic factors are determined controlling the quality appearances on the processed images, which are the lithologic homogeneity, percent of each lithology in the mixed facies, rock unit thickness, outcrop width, weathering intensity, surficial sediment covers, which part of the unit is exposed, and topographic occurrence of the unit. Some band ratios can bind some of these factors and present the rock unit as clear uniform image color and the other show the unit having multicolor. Anyway, the previous geologic interpretation for the processed ratios could be acquired more precession so, the present interpretation defined the band ratio quality of each lithologic unit by three orders of quality. The first order quality that defines here a lithologic unit, it may be changed into the present second and/or third order ratio in the definition the same lithology in other areas.

Geologic setting

The study area represents the northern end of the Nile Valley (Fig. 1), it is bounded from the east by the Oligo-Miocene Gulf of Suez rifting and from the west by the flat-lying Tertiary units that are unconformably rest on the highly deformed Jurassic-Cretaceous units. The deformation of

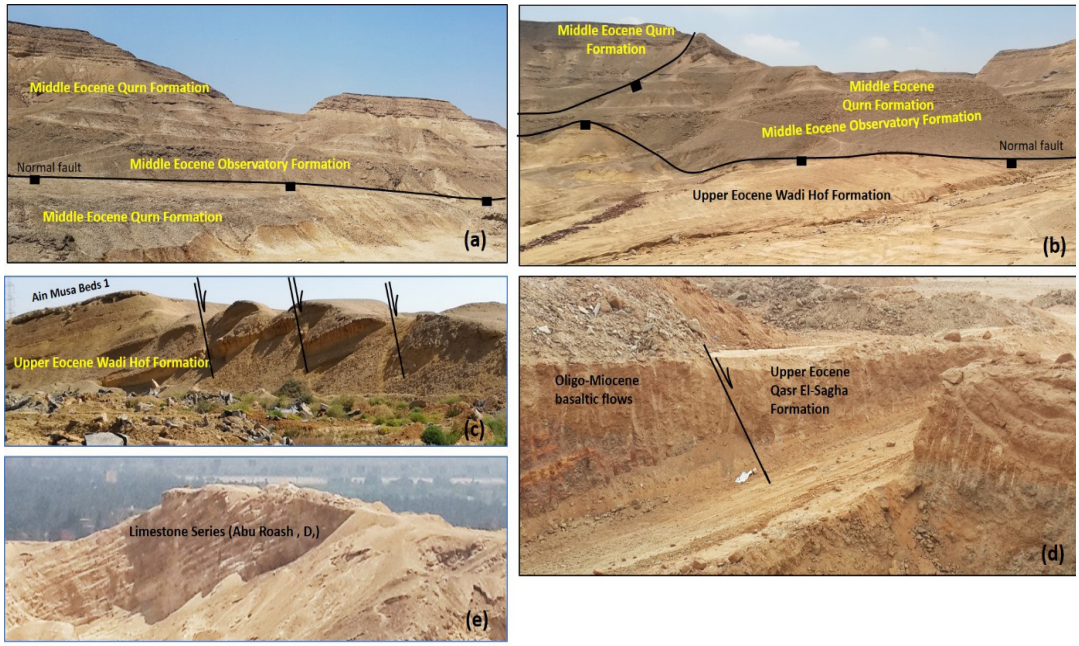

Fig. 12. Field photographs showing the structures affecting the Middle Eocene units in the eastern side (a), the Middle-Upper Eocene rock units in the eastern side (b), the Upper Eocene Wadi Hof Formation in the eastern side (c), the basaltic flows in the western side (d), the limb of Ghigaga anticline in the western side (e).

these rock units is considered belonging to the Syrian Arc tectonic events by many authors (Moustafa, 1988; Moustafa et al., 1998; Hussein and Abd-Allah, 2001 among them). Two of the most pervasive grains of this deformation are the deep-seated El Kattaniya high and the exposed Abu Roash deformed Upper Cretaceous rocks.

Detailed remote sensing analyses supplemented by field checks, observations, and measurements (Fig. 12) reveal that the Upper Cretaceous-Quaternary rocks are exposed in the study area. The Middle Eocene-Oligocene rocks building up the eastern side and the Upper Cretaceous-Pliocene rocks made up the western side, both sides are separated by the Pliocene-Quaternary sediments (Fig. 6).

The exposed rocks in the eastern side are almost horizontal, except some dipping units that are mainly related to the displacements on the affecting fault planes. On contrary, the rocks outcropped on the western side show different dipping attitudes, from steep to gentle dipping beds and folds in the Abu Roash area (measured between 8° to nearly vertical, with 13° to 26° majority) (Fig. 12e) to gentle dipping Eocene-Miocene units forming Qasr El-Sagha cuesta (up to 5°) that lying just to the north of the Qarun lake (Fig. 6 cross section A3-B3). The other rock units showing horizontal setting.

The Upper Cretaceous rocks in the Abu Roash area were deformed mainly by two northeast trending anticlines (Fig. 6). These two anticlines (Ghigaga to the north and Wadi Talun to the south) are intervened by Sudr El Khamis syncline. Generally, the beds forming these two anticlines have dip amount ranging from 8° to 25° (Fig. 12e). Several small folds are also observed within the deformed rocks having mainly the same orientations as the major large folds, they are suggested here their development to the flexural slip folding and folds related faulting. The folds in the Abu Roash area are dissected by four sets of faults, which area northwest, northeast, east-northeast, and north-northwest sets in a descending order. The long northwest and northeast striking faults are considered here as axis-perpendicular and axis-parallel faults. the small northwest and north-northwest faults are considered here tear faults affecting the limbs of the major folds. The most important fault is the long east-northeast fault that affects the northern end of the northern anticline (Fig. 6 cross section A2-B2, Ghigaga anticline). Mustafa (1988) revealed that the Late Cretaceous dextral transpression on the plane of this fault was responsible for the formation of the two large folds that extend northeastward belong the whole Abu Roash area and their affecting fault sets.

The Eocene-Miocene rocks lying to the south

of the Abu Roash area rest unconformably on the Upper Cretaceous rocks as well as they are separated by at least two unconformity surfaces at the ends of Upper Eocene and Oligocene units (Fig. 2). The Pliocene-Quaternary sediments rest unconformably on the Middle Eocene rocks inside El Fayum depression (Fig. 6, cross sections A2-B2 and A3-B3).

The Middle Eocene-Pliocene rocks in the western side of the study area are affected mainly by east-west and northwest faults. The east-west faults dissect the Upper Eocene-Miocene rocks lying to the north of El Fayum depression. These normal faults have mainly south-dipping plane that show a predominated normal-slip with slightly dextral component only on two planes (Fig. 12d). these faults affecting Qasr El-Sagha cuesta and could be responsible for the uprising of the basaltic lava in the before the deposition of the Miocene rocks (Fig. 6, cross section A3-A3). As two northwest oriented faults are expected (from the rock units juxtaposition and lineament traces) to affect the northern part of El Fayum depression (Fig. 6).

On the eastern side of the study area, the Middle Eocene-Oligocene rock are highly dissected by northwest and east-west striking normal faults (Figs. 6 and 12a, b, c). In the northern part of this side, the east-west oriented faults down faulted the Upper Eocene-Oligocene rocks against the Middle Eocene rocks forming the Helwan plateau (Figs. 6 cross section A1-B1 and 12b). The faults have large displacement amounts (up to 75 m due north) and the measured slickenside striations on their plane show mainly predominate normal slip with subordinate dextral component (measured rake angle varying from 72° to 90°). Two east-west trending faults affecting the southern part of the Helwan plateau and expected to extend under the Pliocene-Quaternary sediments filling the Nile Valley to dissect the Middle Eocene rock in the east of El Fayum depression (Fig. 6, cross section A1-B1).

The northwest oriented faults have the longest planes in the study area and affect mainly the northern part of the eastern side (Fig. 6). Inside Helwan plateau, these faults juxtapose the Middle Eocene Quarn Formation against the Middle Eocene Observatory Formation (Fig. 12a), whereas they dissect within the Upper Eocene Wadi Hof Formation in the northern part (Fig. 12c).

The faults affecting the northern part of the eastern side have been considered as the results of dextral wrenching on east-west deep-seated faults occurred twice times after the deposition of the Upper Eocene rocks and after the deposition of the Miocene rocks (Moustafa et al., 1985; Moustafa and Abd-Allah, 1991 and 1992; Hussein and abd-Allah, 2001; and Youssef and Abd-Allah 2003).

Conclusion

The present study is mainly focused on the benefits of using optical Remote sensing data and field verification in geological mapping. The PCA and ICA analysis has been applied on Landsat 8 OLI data and ICA analysis on Sentinel-2A data.

All remote sensing data used in the present study have been subjected pre-processing operation such as radiometric and geometric correction before applying processing methods. Several geologic factors are determined controlling the quality appearances on the processed images, which are the lithologic homogeneity, percent of each lithology in the mixed facies, rock unit thickness, outcrop width, weathering intensity, surficial sediment covers, which part of the unit is exposed, and topographic occurrence of the unit. Three orders of qualities are suggested for the band combination ratios that used in the separation of limestone, limestone mixed facies, sand-sandstone, sandstone mixed facies, basaltic flows, clastic and carbonate mixed facies, agricultural cover, water bodies (Qarun and Wadi Rayan lakes and Nile River). These combination ratios are controlled by the lithologic homogeneity, percents of lithologies in the mixed facies, rock unit thickness, outcrop width, weathering intensity, surficial sediment covers, which part of the unit is exposed, and topographic setting of the unit. The Upper Eocene sandstone and claystone mixed facies are well represented on the ICA images rather than those on the PCA. Generally, the separation of these mixed facies in the western bank is better than that in the eastern bank owing to the recent sediments and weathering products covering the eastern one. The ICA_s images exhibit strong interference between the Oligocene sand and Miocene sand, whereas the PCA_L images show strong interference between the Oligocene sand and Upper Eocene sandstone and mudstone mixed facies. The whole basaltic flows in the study area are discriminated well on most images whereas the large (thick) flow parts are separated only on the PCAL (6/5/3RGB) and ICAs (7/2/11RGB). The agricultural layer and its systems are well traced on the PCAL4/7/3RGB, ICAL3/1/2RGB, and ICAs3/11/5RGB images. The northwest striking faults affecting the

northern part of Helwan plateau are traced with reasonable quality on the ICAL6/7/4RGB and ICAs5/6/2RGB.

The east-west faults that offseted the basaltic sheets are clearly mapped on the PCAL3/1/2RGB, ICAL3/1/2RGB, and ICAL4/7/3 images, as well as they are mapped on the ICAs11/2/12RGB and ICAs3/11/5RGB.

References

Aapo, H., Juha, K. and Erkki, O. (2001) Independent Component Analysis, A Wiley-Interscience, publication *JOHN WILEY & SONS, INC*, Final version of **7** March 2001.

Beadnell, H. J. L. (1902) The Cretaceous region of Abu Roash , near the pyramids of Giza. *Geol. Surv. Egypt:* 48 p.

Beadnell, H. J. L. (1905) The Topography and Geology of the Fayum Province of Egypt. *Survey Department of Egypt*, Cairo. 101.

Blankenhorn, M., (1921) Aegypten, Handbuch der Regionalen Geologie, Bd VII, Abt. **9**, Heft 23, Carl Winters Universitatbuchhandlung, Heidelberg. 244 (in German)

El-Sheshtawi, Y. A. (1979) Petrographical and Petrochemical Studies of the Qatrani Basaltic Rocks: [Dissertation]. *Azhar Univeristy*, Cairo.

Hereher, M.E. (2015) Assessing the dynamics of El-Rayan lakes, Egypt, using remote sensing techniques. *Arabian Journal of Geosciences* **81**, 1931-1938.

Hussein, I.M. and Abd-Allah, A.M.A. (2001) Tectonic evolution of the northeastern part of the African continental margin. *Journal of African Earth Sciences* 33, 49-68.

Faris, M. I. (1948) Contribution to the stratigraphy of Abu Roash and the history of the Upper Cretaceous in Egypt– *Bull. Fac. Sci., Cairo Univ*., **27**: 221: 239.

Marks, L., Salem, A., Welc, F., Nitychoruk, J., Chen, Z., Blaauw, M., Zalat, A., Majecka, A., Szymanek, M., Chodyka, M., Tołoczko-Pasek, A., Sun, Q., Zhao, X. and Jiang, J. (2018) Holocene lake sediments from the Faiyum Oasis in Egypt: a record of environmental and climate change. *Boreas* **47**, 62–79.

Meneisy,M.Y. and Abdelaal, A.Y. (1984) Geochronology of phanerozoic volcanic rocks in Egypt. - *Ain Shams Sci. Bull*., **25**: 248, 163-176.

Jux, U. (1954) Zur Geologie des Kreidegebietes von Abu Roash bei Kairo – *Neues Jb. Geol. U. Palaontol.*, **100** (2): 159 – 207.

Moustafa, A.R. (1988) Wrench tectonic in the north Western Desert of Egypt (Abu Roash area, SW of Cairo). *MERC*, *Ain Shams Univ., Earth Sci. Ser.* **2**,1-16.

Moustafa, A.R., Abd-Allah, A.M.A. (1991) Structural setting of the central part of the Cairo-Suez district. *MERC*, *Ain Shams Univ., Earth Sci. Ser.* **5**, 133-145.

Moustafa, A.R., Abd-Allah, A.M.A. (1992) Transfer zones with en echelon faulting at the northern end of the Suez Rift. *Tectonics* **11**, 499-506.

Moustafa, A.R., El-Badrawy, R., Gibali, H. (1998) Pervasive E-ENE oriented faults in northern Egypt and their effect on the development and inversion of prolific sedimentary basins. *EGPC 14th Exploration and Production Conference, Cairo, Egypt*, pp, 51-67.

Moustafa, A.R., Yehia, M.A., Abdel-Tawab, S. (1985) Structural setting of the area east of Cairo, Maadi, and Helwan. MRC, Ain Shams Univ., Earth Sci. Ser. **5**, 40-64.

Said, R. (1962) The Geology of Egypt. – Amsterdam, *Elsevier, pob. co.,* 377p.

Short, N. M., and Blair, R. w. (1986) Geomorphology from Space: A Global Overview of Regional Landforms. *NASA., Washington, DC*.

Shukri, N.M. and Akmal, M.G. (1953) The geology of Gebel El Nasuri and Gebel El- Anqabiya district. - *Bull. Soc. Grogr*. Egypt, **26**: 243-276.

Strougo, A. and Abdallah, A.M. (1990) Mokattamian Stratigraphy of North Central Eastern Desert (south of Maadi-Qattamiya Road). - *MERC Ain Shams Univ., Earth Sci*. Ser., **4**: 152-175.

Youssef, M.I. and Abd-Allah, A.M.A. (2003) Structural geology of the southeastern segment of the Cairo-Suez district, Egypt. *5th Interna]tional Conference on the Geology of the Middle East, Egypt*, pp: 559-569.

Yusuf, B.L., and Y. He. (2011) Application of hyperspectral imaging sensor to differentiate between the moisture and reflectance of healthy and infected tobacco leaves. African Journal of Agricultural Research, 6(29), 6267-6280.

استخدام بيانات الاستشعار عن بعد في تخريط صخور الكريتاسى إلى الزمن الرابع، منطقة القاهرة الكبرى إلى الفيوم، جنوب مرتفع القطانية، مصر

عبدالناصر رزق أبوزيد [١]، وعلي محمد علي عبدالله [٢]، وعبدالحي علي فراج [٣]

[١] قسم الجيولوجيا، كلية العلوم، جامعة الوادي الجديد، و[٢] قسم الجيولوجيا، كلية العلوم، جامعة عين شمس
و[٣] قسم الجيولوجيا، كلية العلوم، جامعة أسيوط، جمهورية مصر العربية

تضم منطقة الدراسة منطقة الفيوم ومنطقة أبو رواش ومنطقة القاهرة الكبرى وهى ضمن المناطق التى تحيط بمرتفع القطانية من ناحية الجنوب والشرق، وتتميز منطقة الدراسة بالتنوع الشديد في اختلاف السحنات الصخرية حيث انها تتضمن الغطاء الرسوبى من الكريتاسي الأعلى وحتى رواسب الزمن الرابع وكذلك الطفوح البازلتية التى تميز منطقة شرق القاهرة وكذلك منطقة أبو رواش وجبل قطرانى بالفيوم كما انها تتأثر هذه الصخور بمجموعة من التراكيب الجيولوجية المختلفة ونظرا للتنوع في الأنشطة الزراعية علي جانبى نهر النيل وكذلك التنوع فى نوعية المسطحات المائية من مياه عذبة وأخرى تتدرج في ملوحتها كما فى بحيرة قارون وبحيرات وادى الريان، ولما كان في الآونة الأخيرة التقدم فى تقنيات الاستشعار عن بعد والمرئيات الفضائية المنتجة من الاقمار الصناعية المختلفة. ونظرا لهذا التنوع الكبير في منطقة الدراسة فقد استخدمت بيانات المرئيات الفضائية متعددة الأطياف للقمر الصناعي Landsat 8 OLI والقمر الصناعى Sentinel-2A واستخدم تحليل كل من PCA and ICA لفصل الوحدات الجيولوجية ذات السحنات المختلفة وكذلك الغطاء الزراعي والغطاء المائى في منطقة الدراسة، والجديد بالذكر ان هناك العديد من العوامل المؤثرة والمتحكمة في جودة ظهور الوحدات المختلفة على الصور المعالجة ومن هذه العوامل التباين في السحنات الصخرية ونسبة الخلط بين السحنات وبعضها البعض وسمك الوحدات ومدى اتساع المكاشف ومعدلات التجوية المختلفة والوضع الطبوغرافى لها وقد خلصت النتائج الى وجود ثلاثة رتب من جودة خلط الحزم الطيفية المختلفة كناتج لتحليلات كل من PCA and ICA لوحدات الحجر الجيرى، والسحنات المختلطة به، والحجر الرملى والحجر الرملى المختلط بالسحنات الأخرى والطفوح البازلتية والغطاء الزراعى والمائى. وقد أظهرت نتائج تحليل ICA على المرئيات الفضائية وحدات الأيوسين العلوى والمكونة من الحجر الرملى والحجر الطينى المختلط السحنات أكثر وضوحا من نتائج تحليل PCA. كما أوضحت نتائج التحليل PCAL (6/5/3RGB) and ICAs (7/2/11RGB لكل من مرئيات Landsat 8 OLI وSentinel-2A على التوالي الطفوح البازلتية وخاصة الطفوح ذات السمك الكبير. كما أوضحت النتائج PCAL3/1/2RGB, ICAL3/1/2RGB, and ICAL4/7/3 الصدوع التي تأخذ اتجاه شرق – غرب والمتأثر بها الطفوح البازلتية.